Stephen Coombes · Peter beim Graben
Roland Potthast · James Wright *Editors*

Neural Fields

Theory and Applications

Springer

Neural Fields

Stephen Coombes • Peter beim Graben •
Roland Potthast • James Wright
Editors

Neural Fields

Theory and Applications

Springer

Editors
Stephen Coombes
School of Mathematical Sciences
University of Nottingham
Nottingham, United Kingdom

Peter beim Graben
Department of German Studies
and Linguistics
Humboldt-Universität zu Berlin
Berlin, Germany

Roland Potthast
Department of Mathematics
University of Reading
Reading, United Kingdom

James Wright
School of Medicine
University of Auckland
Auckland, New Zealand

ISBN 978-3-642-54592-4 ISBN 978-3-642-54593-1 (eBook)
DOI 10.1007/978-3-642-54593-1
Springer Heidelberg New York Dordrecht London

Library of Congress Control Number: 2014942371

Printed on acid-free paper

Springer is part of Springer Science+Business Media (www.springer.com)

Preface

The Neural Field: A Framework for Brain Data Integration?

This book presents a perspective on the advancing subject of neural fields—that is, theories of brain organization and function in which the interaction of billions of neurons is treated as a continuum. The intention is to reduce the enormous complexity of neuronal interactions to simpler, population properties that are tractable by analytical mathematical tools. By so doing, it is hoped that the theory of brain function can be reduced to its essence, without becoming lost in a wealth of inessential detail. Naturally, this begs the questions of what the "essence" is, and what detail is inessential [1]. The questions themselves are timely for more than neural field theory. Putting aside the most profound of philosophical issues—the existential relation between objective brain function and subjective consciousness—at the cellular level, research has achieved detailed knowledge of individual neuron physiology, and at the gross level, considerable knowledge of sensory processing, the generation of movement and the functional locations in the brain of memory, learning, emotion and decision-making. Yet our knowledge of the functional details of all these processes remains vague, and little surpasses the views held by Sherrington [4]. The ever-accumulating body of experimental data, gathered with ever-improving observational techniques, continues to promise that fundamental understanding of the modes of operation of the brain may be possible—yet the goal seems also to move away, like a mirage, because, despite the mass of data, there is no agreed means to achieve the needed integration. A crisis of confidence looms. It is to be hoped that such a crisis is a healthy state—the darkness before the dawn—analogous to the problems of systematic biology before Darwin, or of astronomy before Kepler, or, more recently, of atomic physics before Bohr, but hope alone will not suffice.

Aware of the risk of becoming trapped in an overwhelming mass of undigested detail, large groups of scientists are joining forces to address the problems of integration. While organizing collaborative efforts of scale unprecedented in neuroscience, all concerned agree on the importance both of technological advances

and of theoretical development, but there are many differences of opinion on the best and shortest route to success. In Europe the *Human Brain Project* [6] is aimed at large scale simulation of the brain, employing very detailed cellular properties. In the United States, the *Brain Activity Map* [5] seeks to establish a functional connectome of the entire brain, and the *MindScope Project* [3] intends to obtain a complete model of the mouse visual cortex. The *BRAIN (Brain Research through Advancing Innovative Neurotechnologies)* Initiative [7] aims to accelerate techniques for study of the brain.

Unresolved questions and fears, around which controversy centres, are:

Do we yet have enough detailed data on structure? How much knowledge of exact connectivity in the brain is enough? Established anatomical techniques are not depleted of possibility to resolve more detail, and very sophisticated new technology is being deployed to add further to this. Yet the capacity of individuals to undergo profound brain damage or deformity of brain development without loss of essential function makes the need for such precise detail seem questionable.

Might some crucial type of data still be missing? Controversy over the role of electrical coupling of neurons, and that of glial cells, over and above signal transmission via axon-synaptic couplings, continues to simmer. Might there be rules of synaptic connection that are not apparent, because the pattern cannot be ascertained within the billions of neurons involved?

To reveal essential patterns of activity, do different types of data have to be obtained using concurrent recording methods? All existing techniques offer a window on brain function limited in scale or in resolution in space or time. That is, only a comparatively few cells can be observed at once, the brain's electric and magnetic fields are relatively blurred in space, and the brain's blood flow, as observed by functional magnetic resonance imaging, is limited to relatively slow variations. None match the scale, speed, and detail relevant to cognition, and the task of making sufficient conjoint observations, in realistic waking contexts, is daunting to say the least.

What then is a reasonably observable explainable unit of the brain? Professor Eric Kandel advocates the complete analysis of a fly or worm brain, as an initial step in the mega-collaborations [2], but in what way, exactly, is a worm's brain more fundamental than, say, a sympathetic ganglion, or a fly's brain than a sensory-motor reflex?

If all the most important observable data is already available, or will become so, will sufficient computer power enable a working brain to be simulated? If this were achieved, would we be any the wiser, or simply unable to understand the functioning of the simulation, just as we cannot understand that upon which the simulation would be based? And would the simulation not, itself, be a person? Thus making our justification for subjecting it to manipulation and interference in the interests of science a little ethically questionable?

Obviously there is no way of knowing the answers to such questions without already having a sufficient unified theoretical understanding of brain function, within which old and new observations can be seen in context. Neural Field Theory hopes to discover such a unification, using as its guiding light explanation of the

large scale observable fields of brain activity, and expecting as this account proceeds an emergent insight into neural information processing. In contrast to its close relative, neural network theory, it seeks explanations beyond the interaction of smaller numbers of neurons, depending instead on the properties of small neural groups to define the properties of the continuum. The layout of this book reflects these intents.

After a brief tutorial, in the first half of the book and beginning from an historical perspective, differing approaches to formulating and analysing equations for neural fields are presented, and in their variety also revealing an underlying unity of conception. Stochastic dynamics are discussed, as well as means of introducing more anatomically and physiologically realistic properties to neural field equations.

The second half of the book begins by addressing the question of embodiment of universal computation within neural fields, and moves on to cognitive processes. Detailed models with cortical connectivity approaching that of the mammalian brain and the relationship to the large-scale electrical fields of the brain follow, and the book concludes with an attempt to show how fundamental field dynamics may play a part in the brain's embryonic development.

Thus a preliminary framework is discernible—methods now exist with the potential to unify material drawn from many branches of neuroscience, guiding their synthesis towards working models that can be tested against observable physical and cognitive properties of the working brain. The framework remains frail, and although the concepts involved seem largely internally consistent, in detail—for instance in the choice of parameters applied in different work—the work reported here is not entirely so. It is not yet possible to say the elusive "essence" referred to in the first paragraph has been captured. But the hopes held at the dawn of this subject appear to have been justified, and future prospects encouraging.

Stephen Coombes
Peter beim Graben
Roland Potthast
James Wright

References

1. Beim Graben, P., Wright, J. J.: From McCulloch-Pitts neurons toward biology. Bull. Math. Biol. **73**, 261–265 (2011)
2. Kandel, E.R., Markram, H., Mathews, P.M., Yuste, R., Koch, C.: Neuroscience thinks big (and collaboratively). Nat. Rev. Neurosci. **14**, 659–664 (2013)
3. nice.sandia.gov/documents/Christof_Koch_SandiaFEB'13.pdf
4. Sherrington, C.S.: Man on His Nature. Gifford Lecture, Edinburgh, 1937–1938. Cambridge University Press, Cambridge (1940)
5. www.columbia.edu/cu/biology/faculty/yuste/bam.html?
6. www.humanbrainproject.eu
7. www.nih.gov/science/brain/

Contents

Chapter 1
Tutorial on Neural Field Theory

Stephen Coombes, Peter beim Graben, and Roland Potthast

Abstract The tools of dynamical systems theory are having an increasing impact on our understanding of patterns of neural activity. In this tutorial chapter we describe how to build tractable tissue level models that maintain a strong link with biophysical reality. These models typically take the form of nonlinear integro-differential equations. Their non-local nature has led to the development of a set of analytical and numerical tools for the study of spatiotemporal patterns, based around natural extensions of those used for local differential equation models. We present an overview of these techniques, covering Turing instability analysis, amplitude equations, and travelling waves. Finally we address inverse problems for neural fields to train synaptic weight kernels from prescribed field dynamics.

1.1 Background

Ever since Hans Berger made the first recording of the human electroencephalogram (EEG) in 1924 [8] there has been a tremendous interest in understanding the physiological basis of brain rhythms. This has included the development of mathematical models of cortical tissue – which are often referred to as neural field models. One of the earliest of such models is due to Beurle [9] in the 1950s, who developed a continuum description of the proportion of active neurons in a randomly connected network. This was followed by work of Griffith [40, 41]

S. Coombes (✉)
School of Mathematical Sciences, University of Nottingham, NG7 2RD Nottingham, UK
e-mail: stephen.coombes@nottingham.ac.uk

P.B. Graben
Bernstein Center for Computational Neuroscience, 10115 Berlin, Germany

R. Potthast
Department of Mathematics, University of Reading, RG6 6AX Reading, UK
Deutscher Wetterdienst, Offenbach, Germany

S. Coombes et al. (eds.), *Neural Fields*, DOI 10.1007/978-3-642-54593-1_1,

in the 1960s, who also published two books that still make interesting reading for modern practitioners of mathematical neuroscience [42, 43]. However, it were Wilson and Cowan [88,89], Nunez [67] and Amari [3] in the 1970s who provided the formulations for neural field models that is in common use today (see Chaps. 2 and 3 in this book). Usually, neural field models are conceived as neural mass models describing population activity at spatiotemporally coarse-grained scales [67, 89]. They can be classified as either activity-based [89] or voltage-based [3, 67] models (see [14, 64] for discussion).

For their activity-based model Wilson and Cowan [88, 89] distinguished between excitatory and inhibitory sub-populations, as well as accounted for refractoriness. This seminal model can be written succinctly in terms of the pair of partial integro-differential equations:

$$\begin{aligned}\frac{\partial E}{\partial t} &= -E + (1 - r_E E) S_E[w_{EE} \otimes E - w_{EI} \otimes I],\\ \frac{\partial I}{\partial t} &= -I + (1 - r_I I) S_I[w_{IE} \otimes E - w_{II} \otimes I].\end{aligned} \tag{1.1}$$

Here $E = E(\mathbf{r}, t)$ is a temporal coarse-grained variable describing the proportion of excitatory cells firing per unit time at position $\mathbf{r}$ at the instant t. Similarly the variable I represents the activity of an inhibitory population of cells. The symbol $\otimes$ represents spatial convolution, the functions $w_{ab}(\mathbf{r})$ describe the weight of all synapses to the ath population from cells of the bth population a distance $|\mathbf{r}|$ away, and r_a is proportional to the refractory period of the ath population (in units of the population relaxation rate). The nonlinear function S_a describes the expected proportion of neurons in population a receiving at least threshold excitation per unit time, and is often taken to have a sigmoidal form. In many modern uses of the Wilson-Cowan equations the refractory terms are often dropped. For exponential or Gaussian choices of the connectivity function the Wilson-Cowan model is known to support a wide variety of solutions, including spatially and temporally periodic patterns (beyond a Turing instability), localised regions of activity (bumps and multi-bumps) and travelling waves (fronts, pulses, target waves and spirals), as reviewed in [19, 20, 32] and in Chaps. 4, 5, 7 or 8.

Further work on continuum models of neural activity was pursued by Nunez [67] and Amari [2, 3] under natural assumptions on the connectivity and firing rate function. Amari focused on local excitation and distal inhibition which is an effective model for a mixed population of interacting inhibitory and excitatory neurons with typical cortical connections (commonly referred to as Mexican hat connectivity), and formulated a single population (scalar) voltage-based model (without refractoriness) for activity $u = u(\mathbf{r}, t)$ of the form

$$\frac{\partial u}{\partial t} = -u + w \otimes f(u), \tag{1.2}$$

for some sigmoidal firing rate function f and connectivity function w. For the case that f is a Heaviside step function he showed how exact results for localised states (bumps and travelling pulses) could be obtained.

Since the original contributions of Wilson, Cowan, Nunez and Amari similar models have been used to investigate a variety of neural phenomena, including electroencephalogram (EEG) and magnetoencephalogram (MEG) rhythms [51, 52, 64, 68] (cf. Chaps. 10, 14, and 17), geometric visual hallucinations [16, 33, 84], mechanisms for short term memory [62, 63], feature selectivity in the visual cortex [7], motion perception [39], binocular rivalry [54], and anaesthesia [65] (cf. Chaps. 14 and 15). Neural field models have also found applications in autonomous robotic behaviour [30] (Chap. 13), embodied cognition [81] (Chap. 12), and Dynamic Causal Modelling [28] (Chap. 17), as well as being studied from an inverse problems perspective [5, 75]. As well as an increase in the applications of models like (1.1) and (1.2) in neuroscience, there has been a push to develop a deeper mathematical understanding of their behaviour. This has led to results in one spatial dimension about the existence and uniqueness of bumps [58] and waves [34] with smooth sigmoidal firing rates, as well as some constructive arguments that generalise the original ideas of Amari for a certain class of smoothed Heaviside firing rate functions [23, 69]. Other mathematical work has focused on geometric singular perturbation analysis as well as numerical bifurcation techniques to analyse solutions in one spatial dimension [62, 72, 73]. More explicit progress has been possible for the case of Heaviside firing rate functions, especially as regards the stability of solutions using Evans functions [22]. The extension of results from one to two spatial dimensions has increased greatly in recent years [24,37,56,60,61,70,85] (see Chap. 7). This style of work has also been able to tackle physiological extensions of minimal neural field models to account for axonal delays [21, 48, 50, 67] (included in the original Wilson-Cowan model and then dropped for simplicity), dendritic processing [15], and synaptic depression [55]. In contrast to the analysis of spontaneously generated patterns of activity, relatively little work has been done on neural fields with forcing. The exceptions perhaps being the work in [38] (for localised drive) and global period forcing in [78]. However, much of the above work exploits idealisations of the original models (1.1) and (1.2), especially as regards heterogeneity and noise, to make mathematical progress. More recent work that tackles heterogeneity (primarily using simulations) can be found in [11] (also in Chap. 8), whilst perturbation theory and homogenisation techniques are developed in [13, 24, 80], and functional analytic results in [36]. The treatment of stochastic neural field models is a very new area, and we refer the reader to the recent review by Bressloff [14] and to Chaps. 2 and 9, which also covers methods from non-equilibrium statistical physics that attempt to move beyond the mean-field rate equations of the type exemplified by (1.1) and (1.2). However, it is fair to say that the majority of neural field models in use today can trace their roots back to the seminal work of Wilson and Cowan, Nunez and Amari.

In this chapter we will develop the discussion of a particular neural field model that incorporates much of the spirit of (1.1) and (1.2), though with refinements that make a stronger connection to models of both synaptic and dendritic processing.

We will then show how to analyse these models with techniques from dynamical systems before going on to discuss inverse problems in neural field theory.

1.1.1 Synaptic Processing

At a synapse, presynaptic firing results in the release of neurotransmitters that causes a change in the membrane conductance of the postsynaptic neuron. This postsynaptic current may be written

$$I_s = g(V - V_s), \tag{1.3}$$

where V is the voltage of the postsynaptic membrane, V_s is its reversal potential and g is a conductance. This is proportional to the probability that a synaptic receptor channel is in an open conducting state. This probability depends on the presence and concentration of neurotransmitter released by the presynaptic neuron. The sign of V_s relative to the resting potential (assumed to be zero) determines whether the synapse is excitatory ($V_s > 0$) or inhibitory ($V_s < 0$).

The effect of some synapses can be described with a function that fits the shape of the postsynaptic response due to the arrival of action potential at the presynaptic release site. A postsynaptic conductance change $g(t)$ would then be given by

$$g(t) = \overline{g}\eta(t - T), \qquad t \geq T, \tag{1.4}$$

where T is the arrival time of a presynaptic action potential and $\eta(t)$ fits the shape of a realistic postsynaptic conductance. A common (normalised) choice for $\eta(t)$ is a difference of exponentials:

$$\eta(t) = \left(\frac{1}{\alpha} - \frac{1}{\beta}\right)^{-1} [\mathrm{e}^{-\alpha t} - \mathrm{e}^{-\beta t}]H(t), \tag{1.5}$$

or the α-function:

$$\eta(t) = \alpha^2 t \mathrm{e}^{-\alpha t} H(t), \tag{1.6}$$

where H is a Heaviside step function. The conductance change arising from a train of action potentials, with firing times T_m, is given by

$$g(t) = \overline{g} \sum_m \eta(t - T_m). \tag{1.7}$$

We note that both the forms for $\eta(t)$ above can be written as the Green's function of a linear differential operator, so that $Q\eta = \delta$, where

$$Q = \left(1 + \frac{1}{\alpha}\frac{\mathrm{d}}{\mathrm{d}t}\right)\left(1 + \frac{1}{\beta}\frac{\mathrm{d}}{\mathrm{d}t}\right), \tag{1.8}$$

for (1.5) and one simply sets $\beta = \alpha$ to obtain the response describing an α-function.

1.1.2 Dendritic Processing

Dendrites form the major components of neurons. They are complex branching structures that receive and process thousands of synaptic inputs from other neurons. It is well known that dendritic morphology plays an important role in the function of dendrites. A nerve fibre consists of a long thin, electrically conducting core surrounded by a thin membrane whose resistance to transmembrane current flow is much greater than that of either the internal core or the surrounding medium. Injected current can travel long distances along the dendritic core before a significant fraction leaks out across the highly resistive cell membrane. Conservation of electric current in an infinitesimal cylindrical element of nerve fibre yields a second-order linear partial differential equation (PDE) known as the *cable equation*. Let $V(x,t)$ denote the membrane potential at position x along a uniform cable at time t measured relative to the resting potential of the membrane. Let τ be the cell membrane time constant, λ the space constant and r the membrane resistance, then the basic uniform (infinite) cable equation is

$$\tau\frac{\partial V(x,t)}{\partial t} = -V(x,t) + \lambda^2\frac{\partial^2 V(x,t)}{\partial x^2} + rI(x,t), \quad x \in (-\infty,\infty), \tag{1.9}$$

where we include the source term $I(x,t)$ corresponding to external input injected into the cable. diffusion along the dendritic tree generates an effective spatiotemporal distribution of delays as expressed by the associated Green's function of the cable equation in terms of the diffusion constant $D = \lambda^2/\tau$. In response to a unit impulse at x' at $t = 0$ and taking $V(x,0) = 0$ the dendritic potential behaves as $V(x,t) = G_\infty(x - x', t)$, where

$$G_\infty(x,t) = \frac{1}{\sqrt{4\pi Dt}}\mathrm{e}^{-t/\tau}\mathrm{e}^{-x^2/(4Dt)}H(t). \tag{1.10}$$

The Green's function $G_\infty(x,t)$ (derived in Appendix 1) determines the linear response to an instantaneous injection of unit current at a given point on the tree. Using the linearity of the cable equation one may write the general solution as

$$\begin{aligned} V(x,t) = &\int_{-\infty}^{t}\mathrm{d}t'\int_{-\infty}^{\infty}\mathrm{d}x' G_\infty(x - x', t - t')I(x',t') \\ &+ \int_{-\infty}^{\infty}\mathrm{d}x' G_\infty(x - x', t)V(x',0). \end{aligned} \tag{1.11}$$

Note that for notational simplicity we have absorbed a factor of r/τ within the definition of the source term $I(x,t)$. For example, assuming the soma is at $x = 0$, $V(x,0) = 0$ and the synaptic input is a train of spikes at $x = x'$, $I(x,t) = \delta(x - x')\sum_m \delta(t - T_m)$ we have that

$$V(0,t) = \sum_m G_\infty(x', t - T_m). \tag{1.12}$$

1.2 Tissue Level Firing Rate Models with Axo-Dendritic Connections

At heart modern biophysical theories assert that EEG signals from a single scalp electrode arise from the coordinated activity of $\sim 10^6$ pyramidal cells in cortex [27]. These are arranged with their dendrites in parallel and perpendicular to the cortical surface. When synchronously activated by synapses at the proximal dendrites extracellular current flows (parallel to the dendrites), with a net membrane current at the synapse. For excitatory (inhibitory) synapses this creates a sink (source) with a negative (positive) extracellular potential. Because there is no accumulation of charge in the tissue the proximal synaptic current is compensated by other currents flowing in the medium causing a distributed source in the case of a sink and vice-versa for a synapse that acts as a source. Hence, at the population level the potential field generated by a synchronously activated population of cortical pyramidal cells behaves like that of a dipole layer. Although the important contribution that single dendritic trees make to generating extracellular electric field potentials has been realised for some time, and can be calculated using Maxwell equations [71], they are typically not accounted for in neural field models. The exception to this being the work of Bressloff, reviewed in [15] and in Chap. 10.

In many neural population models it is assumed that the interactions are mediated by firing rates rather than action potentials (spikes) per se. To see how this might arise we rewrite (1.7) in the equivalent form

$$Qg = \overline{g}\sum_m \delta(t - T_m). \tag{1.13}$$

If we perform a short-time average of (1.13) over some time-scale Δ and assume that η is sufficiently *slow* so that $\langle Qg\rangle_t$ is approximately constant, where

$$\langle x\rangle_t = \frac{1}{\Delta}\int_{t-\Delta}^{t} x(s)\mathrm{d}s, \tag{1.14}$$

then we have that $Qg = f$, where f is the instantaneous firing rate (number of spikes per time Δ). For a single neuron (real or synthetic) experiencing a constant drive it is natural to assume that this firing rate is a function of the drive alone. If for

the moment we assume that a neuron spends most of its time close to rest such that $V_s - V \approx V_s$, and absorb a factor V_s into g, then for synaptically interacting neurons this drive is directly proportional to the conductance state of the presynaptic neuron. Thus for a single population with self-feedback we are led naturally to equations like:

$$Qg = w_0 f(g), \tag{1.15}$$

for some strength of coupling w_0. A common choice for the *population* firing rate function is the sigmoid

$$f(g) = \frac{1}{1 + \exp(-\beta(g - h))}, \tag{1.16}$$

which saturates to one for large g. This functional form, with threshold h and steepness parameter β, is approximately obtained for a unimodal distribution of firing thresholds among the population [88]. Note that the notion of a slow response would also be expected in a large globally coupled network which was firing asynchronously (so that mean field signals would be nearly constant).

To obtain a tissue level model in one spatial dimension we simply consider $g = g(x, t)$, with $x \in \mathbb{R}$, and introduce a coupling function and integrate over the domain to obtain

$$Qg = \int_{-\infty}^{\infty} w(x, y) f(g(y, t - D(x, y)/v))\mathrm{d}y, \tag{1.17}$$

or equivalently

$$g(x, t) = \int_{-\infty}^{t} \mathrm{d}s \eta(t - s) \int_{-\infty}^{\infty} w(x, y) f(g(y, s - D(x, y)/v))\mathrm{d}y. \tag{1.18}$$

Here we have allowed for a communication delay, that arises because of the finite speed, v, of the action potential, where $D(x, y)$ measures the length of the axonal fibre between points at x and y. The coupling function $w(x, y)$ represents anatomical connectivity, and is often assumed to be homogeneous so that $w(x, y) = w(|x - y|)$. It is also common to assume that $D(x, y) = |x - y|$.

Following the original work of Bressloff (reviewed in [15]) we now develop the cable modelling approach of Rall [82] to describe a firing rate cortical tissue model with axo-dendritic patterns of synaptic connectivity. For simplicity we shall consider only an effective single population model in one (somatic) spatial dimension to include a further dimension representing position along a (semi-infinite) dendritic cable. The firing rate in the somatic (cell body) layer is taken to be a smooth function of the cable voltage at the soma, which is in turn determined by the spatiotemporal pattern of synaptic currents on the cable. For an illustration see Fig. 1.1.

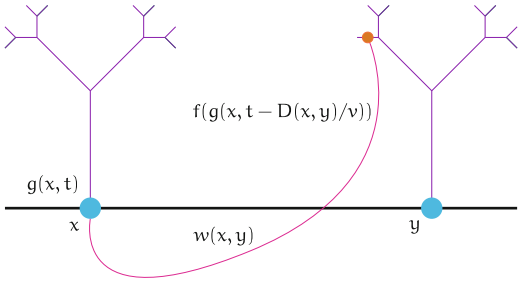

Fig. 1.1 Diagram of a one dimensional neural field model. In this illustration the dendritic tree is drawn with a branched structure. For the sake of simplicity the neural field model is only developed here for unbranched dendrites. However, this can be naturally generalised using the "sum-over-trips" approach of Abbott et al. for passive dendrites [1] and Coombes et al. [25] for resonant dendrites

The voltage $V(\xi, x, t)$ at position $\xi \geq 0$ along a semi-infinite passive cable with somatic coordinate $x \in \mathbb{R}$ can then be written:

$$\frac{\partial V}{\partial t} = -\frac{V}{\tau} + D\frac{\partial^2 V}{\partial \xi^2} + I(\xi, x, t). \tag{1.19}$$

Here, $I(\xi, x, t)$ is the synaptic input (and remember that we absorb within this a factor r/τ), and we shall drop shunting effects and take this to be directly proportional to a conductance change, which evolves according to the usual neural field prescription (cf. Eq. (1.18)) as

$$g(\xi, x, t) = \int_{-\infty}^{t} \mathrm{d}s\eta(t-s) \int_{-\infty}^{\infty} \mathrm{d}y W(\xi, x, y) f(h(y, s - D(x, y)/v)). \tag{1.20}$$

The function $W(\xi, x, y)$ describes the axo-dendritic connectivity pattern and the field h is taken as a measure of the drive at the soma. As a simple model of h we shall take it to be the somatic potential and write $h(x, t) = V(0, x, t)$. For no flux boundary conditions $\partial V(\xi, x, t)/\partial \xi|_{\xi=0} = 0$, and assuming vanishing initial data, the solution to (1.19) at $\xi = 0$ becomes

$$V(\xi = 0, x, t) = \kappa(G \otimes g)(\xi = 0, x, t), \quad G = 2G_\infty \tag{1.21}$$

for some constant of proportionality $\kappa > 0$, where $G_\infty(x, t)$ is given by (1.10) and here the operator $\otimes$ denotes spatiotemporal convolution over the (ξ, t) coordinates. Note that in obtaining (1.21) we have used the result that the Green's function (between two points ξ and ξ') for the semi-infinite cable with no flux boundary conditions can be written as $G_\infty(\xi - \xi', t) + G_\infty(\xi + \xi', t)$ [1, 86].

Further assuming that the axo-dendritic weights can be decomposed in the product form $W(\xi, x, y) = P(\xi)w(|x - y|)$ then the equation for h takes the form

$$h(x,t) = \kappa \int_{-\infty}^{t} \mathrm{d}sF(t-s) \int_{-\infty}^{s} \mathrm{d}s'\eta(s-s') \int_{-\infty}^{\infty} \mathrm{d}yw(|x-y|) f(h(y,s'-D(x,y)/v)), \tag{1.22}$$

where

$$F(t) = \int_{0}^{\infty} \mathrm{d}\xi P(\xi)G(\xi,t). \tag{1.23}$$

We regard Eq. (1.22) as a natural extension of the Amari model (1.2) to include synaptic and dendritic processing as well as axonal delays. Note that the Amari model is recovered from (1.22) in the limit $v \to \infty$, $\eta(t) = \mathrm{e}^{-t}H(t)$, and $F(t) = \delta(t)/\kappa$.

1.2.1 Turing Instability Analysis

To assess the pattern forming properties of the model given by (1.22) it is useful to perform a Turing instability analysis. This describes how a spatially homogeneous state can become unstable to spatially heterogeneous perturbations, resulting in the formation of periodic patterns. To illustrate the technique consider the one-dimensional model without dendrites or axonal delays, obtained in the limit $v \to \infty$ and $F(t) \to \delta(t)$:

$$h(x,t) = \kappa \int_{0}^{\infty} \mathrm{d}s\eta(s) \int_{-\infty}^{\infty} \mathrm{d}yw(|y|) f(h(x-y,t-s)). \tag{1.24}$$

One solution of the neural field equation is the spatially uniform resting state $h(x,t) = h_0$ for all x, t, defined by

$$h_0 = \kappa f(h_0) \int_{-\infty}^{\infty} w(|y|)\mathrm{d}y. \tag{1.25}$$

Here we have used the fact that η is normalised, namely that $\int_0^\infty \mathrm{d}s\eta(s) = 1$. We linearise about this state by letting $h(x,t) \to h_0 + h(x,t)$ so that $f(h) \to f(h_0) + f'(h_0)u$ to obtain

$$h(x,t) = \kappa\beta \int_{0}^{\infty} \mathrm{d}s\eta(s) \int_{-\infty}^{\infty} \mathrm{d}yw(y)h(x-y,t-s), \qquad \beta = f'(h_0). \tag{1.26}$$

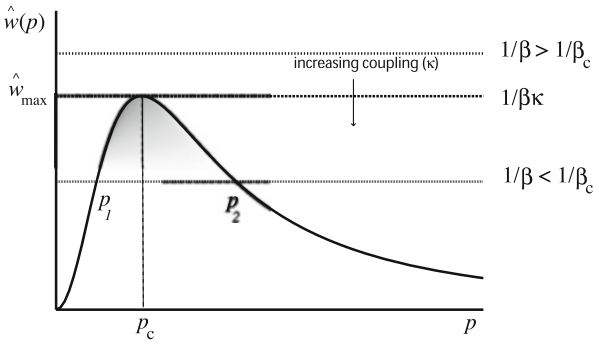

Fig. 1.2 A plot of the Fourier transform of the weight kernel $\hat{w}(p)$ illustrating how its shape (with a maximum away from the origin) can determine a Turing instability defined by the condition $\kappa\beta\hat{w}(p_c) = 1$

This has solutions of the form $e^{\lambda t}e^{ipx}$, with a dispersion curve:

$$1 = \kappa\beta\tilde{\eta}(\lambda)\hat{w}(p), \qquad \hat{w}(p) = \int_{-\infty}^{\infty} dy w(|y|)e^{-ipy}, \qquad \tilde{\eta}(\lambda) = \int_0^{\infty} ds\eta(s)e^{-\lambda s}. \tag{1.27}$$

We recognise $\hat{w}$ as the Fourier transform of w and $\tilde{\eta}$ as the Laplace transform of η. The uniform steady state is linearly stable if $\mathrm{Re}\lambda(p) < 0$ for all $p \in \mathbb{R}$, $p \neq 0$. For the choice $\eta(t) = \alpha e^{-\alpha t}H(t)$ (so that $Q = (1 + \alpha^{-1}d/dt)$) then $\tilde{\eta}(\lambda) = (1 + \lambda/\alpha)^{-1}$. In this case, since $w(x) = w(-x)$ then $\hat{w}(p)$ is a real even function of p and the stability condition is simply

$$\hat{w}(p) < \frac{1}{\beta\kappa}, \qquad \text{for all } \; p \in \mathbb{R}, \quad p \neq 0. \tag{1.28}$$

Now consider the case that $\hat{w}(p)$ has a positive maximum $\hat{w}_{\max}$ at $p = \pm p_c$, that is $\hat{w}(p_c) = \hat{w}_{\max}$ and $\hat{w}(p) < \hat{w}_{\max}$ for all $p \neq p_c$. For $\beta < \beta_c$, where $\beta_c = 1/(\kappa\hat{w}_{\max})$, we have $\kappa\hat{w}(p) \leq \kappa\hat{w}_{\max} < 1/\beta$ for all p and the resting state is linearly stable. At the critical point $\beta = \beta_c$ (see Fig. 1.2) we have $\beta_c\kappa\hat{w}(p_c) = 1$ and $\beta_c\kappa\hat{w}(p) < 1$ for all $p \neq p_c$. Hence, $\lambda(p) < 0$ for all $p \neq p_c$, but $\lambda(p_c) = 0$. This signals the point of a *static* instability due to excitation of the pattern $e^{\pm ip_c x}$. Beyond the bifurcation point, $\beta > \beta_c$, $\lambda(p_c) > 0$ and this pattern grows with time. In fact there will typically exist a range of values of $p \in (p_1, p_2)$ for which $\lambda(p) > 0$, signalling a set of growing patterns. As the patterns grow, the linear approximation breaks down and nonlinear terms dominate the behaviour. The saturating property of f tends to create patterns with finite amplitude, that scale as $\sqrt{\beta - \beta_c}$ close to bifurcation and have wavelength $2\pi/p_c$. If $p_c = 0$ then we would have a *bulk instability* resulting in the formation of another homogeneous state.

A common choice for $w(x)$ is a Mexican hat function which represents short-range excitation and long-range inhibition. An example of such a function is a difference of two exponentials:

$$w(x) = A\left[e^{-\gamma_1|x|} - \Gamma e^{-\gamma_2|x|}\right], \tag{1.29}$$

with $\Gamma < 1$, $\gamma_1 > \gamma_2 > 0$ and $\Lambda = +1$. (The case $\Lambda = -1$, which represents short-range inhibition and long-range excitation will be considered below in the full model.) The Fourier transform $\hat{w}(p)$ is calculated as:

$$\hat{w}(p) = 2\Lambda\left[\frac{\gamma_1}{\gamma_1^2 + p^2} - \Gamma\frac{\gamma_2}{\gamma_2^2 + p^2}\right], \tag{1.30}$$

from which we may determine p_c as

$$p_c^2 = \frac{\gamma_1^2\sqrt{\Gamma\gamma_2/\gamma_1} - \gamma_2^2}{1 - \sqrt{\Gamma\gamma_2/\gamma_1}}. \tag{1.31}$$

Hence, $p_c \neq 0$ when $\Gamma > (\gamma_2/\gamma_1)^3$. Note that for $\Lambda = -1$ then $p_c = 0$ and a static Turing instability does not occur.

For the full model (1.22) with $D(x, y) = |x - y|$ the homogeneous steady state, $h(x, t) = h_0$ for all x, t, satisfies

$$h_0 = \kappa f(h_0)\int_0^\infty F(s)\mathrm{d}s\int_{-\infty}^\infty \mathrm{d}y w(|y|), \tag{1.32}$$

and the spectral equation takes the form

$$1 = \kappa\beta\hat{w}(p, \lambda)\tilde{\eta}(\lambda)\tilde{F}(\lambda), \quad \hat{w}(p, \lambda) = \int_{-\infty}^\infty \mathrm{d}y w(|y|)\mathrm{e}^{-ipy}\mathrm{e}^{-\lambda|y|/v}, \quad \beta = f'(h_0). \tag{1.33}$$

Compared to (1.27) it is now possible for complex solutions for λ to be supported – allowing for the possibility of *dynamic* (as opposed to static) Turing instabilities to occur. These occur when $\mathrm{Im}\,\lambda \neq 0$ at the bifurcation point.

For example, in the limit $v \to \infty$ then $\hat{w}(p, \lambda) \to \hat{w}(p)$ and for $\eta(t) = \alpha\mathrm{e}^{-\alpha t}H(t)$ we have that

$$1 + \lambda/\alpha = \kappa\beta\hat{w}(p)\tilde{F}(\lambda). \tag{1.34}$$

A necessary condition for a dynamic instability ($\mathrm{Re}\,\lambda = 0$ and $\mathrm{Im}\,\lambda \neq 0$) is that there exists a pair ω, $p \neq 0$ such that

$$1 + i\omega/\alpha = \kappa\beta\hat{w}(p)\tilde{F}(i\omega). \tag{1.35}$$

Equating real and imaginary parts (and using the fact that $\hat{w}(p) \in \mathbb{R}$) gives us the pair of simultaneous equations

$$1 = \kappa\beta\hat{w}(p)C(\omega), \qquad \omega/\alpha = \kappa\beta\hat{w}(p)S(\omega), \tag{1.36}$$

where $C(\omega) = \mathrm{Re}\,\tilde{F}(i\omega)$ and $S(\omega) = \mathrm{Im}\,\tilde{F}(i\omega)$. Note that $C(\omega) = \int_0^\infty \mathrm{d}s F(s)\cos(\omega s) \leq |C(0)|$. Hence (dividing the above equations) if there is a non-zero solution to

$$\frac{\omega_c}{\alpha} = \mathscr{H}(\omega_c), \qquad \mathscr{H}(\omega_c) \equiv \frac{S(\omega_c)}{C(\omega_c)}, \tag{1.37}$$

then the bifurcation condition, $\beta = \beta_d$, for a dynamic instability is defined by

$$\beta_d \kappa \hat{w}(p_{\min}) = \frac{1}{C(\omega_c)}, \tag{1.38}$$

which should be contrasted with the bifurcation condition, $\beta = \beta_s$, for a static instability, namely

$$\beta_s \kappa \hat{w}(p_{\max}) = \frac{1}{C(0)}, \tag{1.39}$$

where

$$\hat{w}(p_{\min}) = \min_p \hat{w}(p), \qquad \hat{w}(p_{\max}) = \max_p \hat{w}(p). \tag{1.40}$$

Assuming that $\hat{w}(p_{\min}) < 0 < \hat{w}(p_{\max})$, a dynamic Turing instability will occur if $\beta < \beta_s$ and $p_{\min} \neq 0$, whereas a static Turing instability will occur if $\beta_s < \beta$ and $p_{\max} \neq 0$.

For the Mexican hat function (1.29) with $\Lambda = +1$ (short-range excitation, long-range inhibition), a dynamic Turing instability is not possible since $p_{\min} = 0$. However, it is possible for bulk oscillations to occur instead of static patterns when

$$\hat{w}(p_c) < -\frac{C(\omega_c)}{C(0)}|\hat{w}(0)|, \tag{1.41}$$

with p_c given by (1.31). On the other hand, when $\Lambda = -1$ (short-range inhibition, long-range excitation) a dynamic instability can occur since $p_{\min} = p_c$ and $p_{\max} = 0$, provided that

$$\hat{w}(0) < -\frac{C(\omega_c)}{C(0)}|\hat{w}(p_c)|. \tag{1.42}$$

As an explicit example consider the choice $P(\xi) = \delta(\xi - \xi_0)$ (so that the synaptic contact occurs at a fixed distance $\xi_0 > 0$ from the soma). In this case $F(t) = G(\xi_0, t)$ with Laplace transform (calculated in Appendix 2):

$$\tilde{F}(\lambda) = \frac{\mathrm{e}^{-\gamma(\lambda)\xi_0}}{D\gamma(\lambda)}, \qquad \gamma^2(\lambda) = (1/\tau + \lambda)/D. \tag{1.43}$$

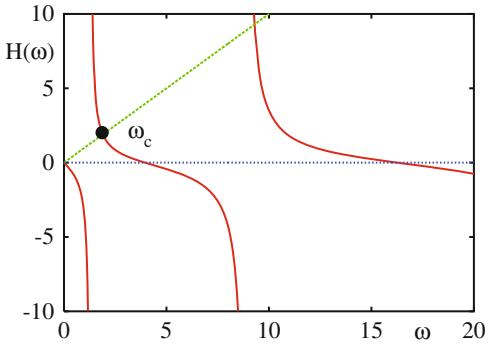

Fig. 1.3 A plot of the function $H(\omega)$ for $D = \tau = 1$ with $\xi_0 = 2$, showing a non-zero solution of (1.37) for $\alpha = 1$. This highlights the possibility of a dynamic Turing instability ($\omega_c \neq 0$) in a dendritic neural field model with short-range inhibition and long-range excitation

In this case we may calculate the real and imaginary parts of $\tilde{F}(i\omega)$ as

$$C(\omega) = \frac{1}{\sqrt{1/\tau^2+\omega^2}} e^{-A_+(\omega)\xi_0}[A_+(\omega)\cos(A_-(\omega)\xi_0) - A_-(\omega)\sin(A_-(\omega)\xi_0)] \tag{1.44}$$

$$S(\omega) = -\frac{1}{\sqrt{1/\tau^2+\omega^2}} e^{-A_+(\omega)\xi_0}[A_+(\omega)\sin(A_-(\omega)\xi_0) + A_+(\omega)\cos(A_-(\omega)\xi_0)], \tag{1.45}$$

where $\sqrt{(1/\tau + i\omega)/D} = A_+(\omega) + iA_-(\omega)$ and

$$A_\pm(\omega) = \sqrt{[\sqrt{1/(\tau D)^2 + \omega^2/D^2} \pm 1/(\tau D)]/2}. \tag{1.46}$$

A plot of $H(\omega)$ is shown in Fig. 1.3, highlighting the possibility of a non-zero solution of (1.37) for a certain parameter set (and hence the possibility of a dynamic instability).

For a discussion of dynamic Turing instabilities with finite v we refer the reader to [87]. For the treatment of more general forms of axo-dendritic connectivity (that do not assume a product form) we refer the reader to [12, 17].

The extension of the above argument to two dimensions shows that the linearised equations of motion have solutions of the form $e^{\lambda t}e^{i\mathbf{p}\cdot\mathbf{r}}$, $\mathbf{r}, \mathbf{p} \in \mathbb{R}^2$, with $\lambda = \lambda(p)$, $p = |\mathbf{p}|$ as determined by (1.33) with

$$\hat{w}(p,\lambda) = \int_{\mathbb{R}^2} d\mathbf{r} w(|\mathbf{r}|) e^{-i\mathbf{p}\cdot\mathbf{r}} e^{-\lambda|\mathbf{r}|/v}. \tag{1.47}$$

Near bifurcation we expect spatially periodic solutions of the form $\exp i[p_1 x + p_2 y]$, $p_c^2 = p_1^2 + p_2^2$. For a given p_c there are an infinite number of choices for p_1 and p_2. It is therefore convenient to restrict attention to doubly periodic solutions that tessellate the plane. These can be expressed in terms of the basic symmetry groups of

hexagon, square and rhombus. Solutions can then be constructed from combinations of the basic functions $e^{ip_c\mathbf{R}\cdot\mathbf{r}}$, for appropriate choices of the basis vectors $\mathbf{R}$. If ϕ is the angle between two basis vectors $\mathbf{R}_1$ and $\mathbf{R}_2$, we can distinguish three types of lattice according to the value of ϕ: square lattice ($\phi = \pi/2$), rhombic lattice ($0 < \phi < \pi/2$) and hexagonal ($\phi = \pi/3$). Hence, all doubly periodic functions may be written as a linear combination of plane waves

$$h(\mathbf{r}) = \sum_j A_j e^{ip_c\mathbf{R}_j\cdot\mathbf{r}} + \text{cc}, \qquad |\mathbf{R}_j| = 1, \tag{1.48}$$

where cc stands for complex-conjugate. For hexagonal lattices we use $\mathbf{R}_1 = (1, 0)$, $\mathbf{R}_2 = (-1, \sqrt{3})/2$, and $\mathbf{R}_3 = (1, \sqrt{3})/2$. For square lattices we use $\mathbf{R}_1 = (1, 0)$, $\mathbf{R}_2 = (0, 1)$, while the rhombus tessellation uses $\mathbf{R}_1 = (1, 0)$, $\mathbf{R}_2 = (\cos\zeta, \sin\zeta)$.

1.2.2 Weakly Nonlinear Analysis: Amplitude Equations

A characteristic feature of the dynamics of systems beyond an instability is the slow growth of the dominant eigenmode, giving rise to the notion of a *separation of scales*. This observation is key in deriving the so-called *amplitude equations*. In this approach information about the short-term behaviour of the system is discarded in favour of a description on some appropriately identified slow time-scale. By Taylor-expansion of the dispersion curve near its maximum one expects the scalings $\text{Re}\,\lambda \sim \beta - \beta_c$, $p - p_c \sim \sqrt{\beta - \beta_c}$, close to bifurcation, where β is the bifurcation parameter. Since the eigenvectors at the point of instability are of the type $A_1 e^{i(\omega_c t + p_c x)} + A_2 e^{i(\omega_c t - p_c x)} + \text{cc}$, for $\beta > \beta_c$ emergent patterns are described by an infinite sum of unstable modes (in a continuous band) of the form $e^{\nu_0(\beta-\beta_c)t} e^{i(\omega_c t + p_c x)} e^{ip_0\sqrt{\beta-\beta_c}x}$. Let us denote $\beta = \beta_c + \epsilon^2\delta$ where ϵ is arbitrary and δ is a measure of the distance from the bifurcation point. Then, for small ϵ we can separate the dynamics into fast eigen-oscillations $e^{i(\omega_c t + p_c x)}$, and slow modulations of the form $e^{\nu_0\epsilon^2 t} e^{ip_0\epsilon x}$. If we set as further independent variables $\tau = \epsilon^2 t$ for the modulation time-scale and $\chi = \epsilon x$ for the long-wavelength spatial scale (at which the interactions between excited nearby modes become important) we may write the weakly nonlinear solution as $A_1(\chi, \tau)e^{i(\omega_c t + p_c x)} + A_2(\chi, \tau)e^{i(\omega_c t - p_c x)} + \text{cc}$. It is known from the standard theory [47] that weakly nonlinear solutions will exist in the form of either travelling waves ($A_1 = 0$ or $A_2 = 0$) or standing waves ($A_1 = A_2$).

We are now in a position to derive the amplitude equations for patterns emerging beyond the point of an instability for a neural field model. These are also useful for determining the sub- or super-critical nature of the bifurcation. For clarity we shall first focus on the case of a static instability, and consider the example system given by (1.18) with $\eta(t) = e^{-t}H(t)$ and $v \to \infty$, equivalent to the Amari model (1.2). In this case the model is conveniently written as an integro-differential equation:

$$\frac{\partial g}{\partial t} = -g + w \otimes f(g), \tag{1.49}$$

where the symbol $\otimes$ denotes spatial convolution (assuming $w(x, y) = w(|x - y|)$).

We first Taylor expand the nonlinear firing rate around the steady state g_0:

$$f(g) = f(g_0) + \beta_1(g - g_0) + \beta_2(g - g_0)^2 + \beta_3(g - g_0)^3 + \ldots, \tag{1.50}$$

where $\beta_1 = f'(g_0)$, $\beta_2 = f''(g_0)/2$ and $\beta_3 = f'''(g_0)/6$. We also adopt the perturbation expansion

$$g = g_0 + \epsilon g_1 + \epsilon^2 g_2 + \epsilon^3 g_3 + \ldots . \tag{1.51}$$

After rescaling time according to $\tau = \epsilon^2 t$ and setting $\beta_1 = \beta_c + \epsilon^2 \delta$, where β_c is defined by the bifurcation condition $\beta_c = 1/\hat{w}(p_c)$, we then substitute into (1.49). Equating powers of ϵ leads to a hierarchy of equations:

$$g_0 = f(g_0) \int_{-\infty}^{\infty} w(|y|) \mathrm{d}y, \tag{1.52}$$

$$0 = \mathscr{L} g_1, \tag{1.53}$$

$$0 = \mathscr{L} g_2 + \beta_2 w \otimes g_1^2, \tag{1.54}$$

$$\frac{\mathrm{d}g_1}{\mathrm{d}\tau} = \mathscr{L} g_3 + \delta w \otimes g_1 + 2\beta_2 w \otimes g_1 g_2 + \beta_3 w \otimes g_1^3, \tag{1.55}$$

where

$$\mathscr{L} g = -g + \beta_c w \otimes g. \tag{1.56}$$

The first equation fixes the steady state g_0. The second equation is linear with solutions $g_1 = A(\tau)\mathrm{e}^{ip_c x} + \mathrm{cc}$ (where p_c is the critical wavenumber at the static bifurcation). Hence the null space of $\mathscr{L}$ is spanned by $\mathrm{e}^{\pm ip_c x}$. A dynamical equation for the complex amplitude $A(\tau)$ (and we do not treat here any slow spatial variation) can be obtained by deriving solvability conditions for the higher-order equations, a method known as the Fredholm alternative. These equations have the general form $\mathscr{L} g_n = v_n(g_0, g_1, \ldots, g_{n-1})$ (with $\mathscr{L} g_1 = 0$). We define the inner product of two periodic functions (with periodicity $2\pi/p_c$) as

$$\langle U, V \rangle = \frac{p_c}{2\pi} \int_0^{2\pi/p_c} U^*(x) V(x) \mathrm{d}x, \tag{1.57}$$

where * denotes complex conjugation. It is simple to show that $\mathscr{L}$ is self-adjoint with respect to this inner product (see Appendix 3), so that

$$\langle g_1, \mathscr{L} g_n \rangle = \langle \mathscr{L} g_1, g_n \rangle = 0. \tag{1.58}$$

Hence we obtain the set of solvability conditions

$$\langle \mathrm{e}^{\pm ip_c x}, v_n \rangle = 0, \qquad n \geq 2. \tag{1.59}$$

The solvability condition with $n = 2$ is automatically satisfied, since $w \otimes g_1^2 = \hat{w}(2p_c)[A^2\mathrm{e}^{2ip_c x} + \mathrm{cc}] + 2|A|^2\hat{w}(0)$, and we make use of the result $\langle \mathrm{e}^{imp_c x}, \mathrm{e}^{inp_c x} \rangle = \delta_{m,n}$. For $n = 3$ the solvability condition (projecting onto $\mathrm{e}^{+ip_c x}$) is

$$\langle \mathrm{e}^{ip_c x}, \frac{\mathrm{d}g_1}{\mathrm{d}\tau} - \delta w \otimes g_1 \rangle = \beta_3 \langle \mathrm{e}^{ip_c x}, w \otimes g_1^3 \rangle + 2\beta_2 \langle \mathrm{e}^{ip_c x}, w \otimes g_1 g_2 \rangle. \tag{1.60}$$

The left-hand side is easily calculated, using $w \otimes g_1 = \hat{w}(p_c)[A\mathrm{e}^{ip_c x} + \mathrm{cc}]$, as

$$\frac{\mathrm{d}A}{\mathrm{d}\tau} - \delta\hat{w}(p_c)A = \frac{\mathrm{d}A}{\mathrm{d}\tau} - \beta_c^{-1}\delta A, \tag{1.61}$$

where we have made use of the bifurcation condition $\beta_c = 1/\hat{w}(p_c)$. To evaluate the right-hand side we use the result that $w \otimes g_1^3 = \hat{w}(p_c)[A^3\mathrm{e}^{i3p_c x} + \mathrm{cc}] + 3|A|^2\hat{w}(p_c)[A\mathrm{e}^{ip_c x} + \mathrm{cc}]$, to obtain

$$\langle \mathrm{e}^{ip_c x}, w \otimes g_1^3 \rangle = 3\beta_c^{-1} A|A|^2. \tag{1.62}$$

The next step is to determine g_2. From (1.54) we have that

$$-g_2 + \beta_c w \otimes g_2 = -\beta_2 \left\{ \hat{w}(2p_c)[A^2\mathrm{e}^{2ip_c x} + \mathrm{cc}] + 2|A|^2\hat{w}(0) \right\}. \tag{1.63}$$

We now set

$$g_2 = A_+\mathrm{e}^{2ip_c x} + A_-\mathrm{e}^{-2ip_c x} + A_0 + \phi g_1. \tag{1.64}$$

The constant ϕ remains undetermined at this order of perturbation but does not appear in the amplitude equation for $A(\tau)$. Substitution into (1.63) and equating powers of $\mathrm{e}^{ip_c x}$ gives

$$A_0 = \frac{2\beta_2|A|^2\hat{w}(0)}{1 - \beta_c\hat{w}(0)}, \quad A_+ = \frac{\beta_2 A^2\hat{w}(2p_c)}{1 - \beta_c\hat{w}(2p_c)}, \quad A_- = A_+^*, \tag{1.65}$$

where we have used the result that $w \otimes g_2 = \hat{w}(2p_c)[A_+\mathrm{e}^{2ip_c x} + A_-\mathrm{e}^{-2ip_c x}] + \hat{w}(0)A_0 + \phi[A\hat{w}(p_c)\mathrm{e}^{ip_c x} + \mathrm{cc}]$. We then find that

$$\langle \mathrm{e}^{ip_c x}, w \otimes g_1 g_2 \rangle = \hat{w}(p_c)[A_+A^* + A_0 A]. \tag{1.66}$$

Combining (1.61), (1.62) and (1.66) we obtain the Stuart-Landau equation

$$\beta_c \frac{\mathrm{d}A}{\mathrm{d}\tau} = A(\delta - \Phi|A|^2), \tag{1.67}$$

where

$$\Phi = -3\beta_3 - 2\beta_2^2\left[\frac{\hat{w}(2p_c)}{1-\beta_c\hat{w}(2p_c)} + \frac{2\hat{w}(0)}{1-\beta_c\hat{w}(0)}\right]. \tag{1.68}$$

Introducing $A = Re^{i\theta}$ we may rewrite Eq. (1.67) as

$$\beta_c\frac{dR}{d\tau} = \delta R - \Phi R^3, \qquad \frac{d\theta}{d\tau} = 0. \tag{1.69}$$

Hence, the phase of A is arbitrary ($\theta = \text{const}$) and the amplitude has a pitchfork bifurcation which is super-critical for $\Phi > 0$ and sub-critical for $\Phi < 0$.

Amplitude equations arising for systems with a dynamic instability are treated in [87]. The appropriate amplitude equations are found to be the coupled mean-field Ginzburg–Landau equations describing a Turing–Hopf bifurcation with modulation group velocity of $O(1)$.

1.2.2.1 Amplitude Equations for Planar Neural Fields

In two spatial dimensions the same ideas go across and can be used to determine the selection of patterns, say stripes vs. spots [31]. In the hierarchy of Eqs. (1.52)–(1.55) the symbol $\otimes$ now represents a convolution in two spatial dimensions. The two dimensional Fourier transform $\hat{w}$ takes the explicit form

$$\hat{w}(p_1, p_2) = \int_{-\infty}^{\infty} dx \int_{-\infty}^{\infty} dy w(x, y)e^{i(p_1x+p_2y)}, \tag{1.70}$$

and the inner product for periodic scalar functions defined on the plane is taken as

$$\langle U, V\rangle = \frac{1}{|\Omega|}\int_{\Omega} U^*(\mathbf{r})V(\mathbf{r})d\mathbf{r}, \tag{1.71}$$

with $\Omega = (0, 2\pi/p_c)\times(0, 2\pi/p_c)$. We shall assume a radially symmetric kernel so that $\hat{w}(p_1, p_2) = \hat{w}\left(\sqrt{p_1^2 + p_2^2}\right)$. One composite pattern that solves the linearised equations is

$$g_1(x, y, \tau) = A_1(\tau)e^{ip_cx} + A_2(\tau)e^{ip_cy} + \text{cc}. \tag{1.72}$$

For $A_1 = 0$ and $A_2 \neq 0$ we have a *stripe*, while if both A_1 and A_2 are non-zero, and in particular equal, we have a *spot*. Here p_c is defined by the condition $\beta_c = 1/\hat{w}(p_c)$. The null space of $\mathscr{L}$ is spanned by $\{e^{\pm ip_cx}, e^{\pm ip_cy}\}$, and we may proceed as for the one dimensional case to generate a set of coupled equations for the amplitudes A_1 and A_2. It is simple to show that

$$\langle e^{ip_cx}, w\otimes g_1^3\rangle = 3\beta_c^{-1}A_1(|A_1|^2 + 2|A_2|^2). \tag{1.73}$$

Assuming a representation for g_2 as

$$g_2 = \alpha_0 + \alpha_1 e^{2ip_c x} + \alpha_2 e^{-2ip_c x} + \alpha_3 e^{2ip_c y} + \alpha_4 e^{-2ip_c y} + \alpha_5 e^{ip_c(x+y)} + \alpha_6 e^{-ip_c(x+y)} + \alpha_7 e^{ip_c(x-y)} + \alpha_8 e^{-ip_c(x-y)} + \phi g_1, \tag{1.74}$$

allows us to calculate

$$\langle e^{ip_c x}, w \otimes g_1 g_2 \rangle = \beta_c^{-1}[\alpha_0 A_1 + \alpha_1 A_1^* + \alpha_5 A_2^* + \alpha_7 A_2]. \tag{1.75}$$

Balancing terms in (1.54) gives

$$\alpha_0 = \frac{2\beta_2(|A_1|^2 + |A_2|^2)\hat{w}(0)}{1 - \beta_c \hat{w}(0)}, \qquad \alpha_1 = \frac{\beta_2 A_1^2 \hat{w}(2p_c)}{1 - \beta_c \hat{w}(2p_c)}, \tag{1.76}$$

$$\alpha_5 = \frac{2\beta_2 A_1 A_2 \hat{w}(\sqrt{2}p_c)}{1 - \beta_c \hat{w}(\sqrt{2}p_c)}, \qquad \alpha_7 = \frac{2\beta_2 A_1 A_2^* \hat{w}(\sqrt{2}p_c)}{1 - \beta_c \hat{w}(\sqrt{2}p_c)}. \tag{1.77}$$

Combining the above yields the coupled amplitude equations:

$$\beta_c \frac{dA_1}{d\tau} = A_1(\delta - \Phi|A_1|^2 - \Psi|A_2|^2), \tag{1.78}$$

$$\beta_c \frac{dA_2}{d\tau} = A_2(\delta - \Phi|A_2|^2 - \Psi|A_1|^2), \tag{1.79}$$

where

$$\Phi = -3\beta_3 - 2\beta_2^2 \left[\frac{2\hat{w}(0)}{1 - \beta_c \hat{w}(0)} + \frac{\hat{w}(2p_c)}{1 - \beta_c \hat{w}(2p_c)} \right], \tag{1.80}$$

$$\Psi = -6\beta_3 - 4\beta_2^2 \left[\frac{\hat{w}(0)}{1 - \beta_c \hat{w}(0)} + \frac{2\hat{w}(\sqrt{2}p_c)}{1 - \beta_c \hat{w}(\sqrt{2}p_c)} \right]. \tag{1.81}$$

The stripe solution $A_2 = 0$ and $|A_1| = \sqrt{\delta/\Phi}$ (or vice versa) is stable if and only if $\Psi > \Phi > 0$. The spot solution $|A_1| = |A_2| = \sqrt{\delta/(\Phi + \Psi)}$ is stable if and only if $\Phi > \Psi > 0$. Hence, stripes and spots are mutually exclusive as stable patterns. In the absence of quadratic terms in f, namely $\beta_2 = 0$, then $\Psi = -6\beta_3$ and $\Phi = -3\beta_3$ so that for an odd firing rate function like $f(x) = \tanh x \simeq x - x^3/3$ then $\beta_3 < 0$ and so $\Psi > \Phi$ and stripes are selected over spots. The key to the appearance of spots is non-zero quadratic terms, $\beta_2 \neq 0$, in the firing rate function; without these terms spots can never stably exist. For a Mexican hat connectivity then $\hat{w}(\sqrt{2}p_c) > \hat{w}(2p_c)$ and the quadratic term of Ψ is larger than that of Φ so that as $|\beta_2|$ increases then spots will arise instead of stripes.

The technique above can also be used to determine amplitude equations for more general patterns of the form

$$g_1(\mathbf{r},\tau) = \sum_{j=1}^{N} A_j(\tau) \mathrm{e}^{ip_c \mathbf{R}_j \cdot \mathbf{r}}. \tag{1.82}$$

For further discussion we refer the reader to [32, 84].

1.2.3 Brain Wave Equations

Given the relatively few analytical techniques for investigating neural field models one natural step is to make use of numerical simulations to explore system dynamics. For homogeneous models we may exploit the convolution structure of interactions to develop fast Fourier methods to achieve this. Indeed we may also exploit this structure further to obtain equivalent PDE models [61] (see also Chap. 5), and recover the brain wave equation often used in EEG modelling [49, 67].

For example consider a one-dimensional neural field model with axonal delays:

$$Qg = \psi, \qquad \psi(x,t) = \int_{-\infty}^{\infty} \mathrm{d}y w(|x-y|) f(g(y, t-|x-y|)/v). \tag{1.83}$$

The function $\psi(x,t)$ may be expressed in the form

$$\psi(x,t) = \int_{-\infty}^{\infty} \mathrm{d}s \int_{-\infty}^{\infty} \mathrm{d}y G(x-y, t-s)\rho(y,s), \tag{1.84}$$

where

$$G(x,t) = \delta(t-|x|/v)w(x), \tag{1.85}$$

can be interpreted as another type of Green's function, and we use the notation

$$\rho(x,t) = f(g(x,t)). \tag{1.86}$$

Introducing Fourier transforms of the following form

$$\psi(x,t) = \frac{1}{(2\pi)^2} \int_{-\infty}^{\infty} \int_{-\infty}^{\infty} \mathrm{e}^{i(kx+\omega t)} \psi(k,\omega) \mathrm{d}k \mathrm{d}\omega, \tag{1.87}$$

allows us to write

$$\psi(k,\omega) = G(k,\omega)\rho(k,\omega), \tag{1.88}$$

assuming the Fourier transform of $f(u)$ exists. It is straightforward to show that the Fourier transform of (1.85) is